

## Microfabricated high-throughput electronic particle detector

D. K. Wood, M. V. Requa, and A. N. Cleland

*Department of Physics, University of California at Santa Barbara, Santa Barbara, California 93106, USA*

(Received 20 June 2007; accepted 14 September 2007; published online 5 October 2007)

We describe the design, fabrication, and use of a radio frequency reflectometer integrated with a microfluidic system, applied to the very high-throughput measurement of micron-scale particles, passing in a microfluidic channel through the sensor region. The device operates as a microfabricated Coulter counter [U.S. Patent No. 2656508 (1953)], similar to a design we have described previously, but here with significantly improved electrode geometry as well as including electronic tuning of the reflectometer; the two improvements yielding an improvement by more than a factor of 10 in the signal to noise and in the diametric discrimination of single particles. We demonstrate the high-throughput discrimination of polystyrene beads with diameters in the 4–10  $\mu\text{m}$  range, achieving diametric resolutions comparable to the intrinsic spread of diameters in the bead distribution, at rates in excess of  $15 \times 10^6$  beads/h. © 2007 American Institute of Physics. [DOI: 10.1063/1.2794230]

### INTRODUCTION

The ability to detect, count, and perform size distribution analyses of living biological cells suspended in aqueous solutions, or more generally the analysis of micron-scale particles in fluid, is an important technology in biology. One of the earliest, and presently most prevalent, technologies for performing this function is embodied in the Coulter counter.<sup>1</sup> In this device, a saline solution, in which the cells or particles are suspended, is passed through a narrow aperture, while monitoring the electrical resistance across the aperture. The presence of a cell or particle in the aperture volume increases the electrical resistance during the time of passage, and this change is detected and recorded. The number of such events observed as a function of time is nearly equal to the number of cells or particles that have passed through the aperture (multiparticle coincident passages give single, albeit larger, signal events, so reduce the total electrical count). Furthermore, the magnitude of the change in resistance during a particle passage is closely related to the diameter of the particle. This technique therefore allows the construction of histograms of particle size distributions, as well as total particle counts. This type of device is commercially available from a number of vendors.

A number of researchers have developed variants on this device, typified by the resistive pulse analyzer,<sup>2,3</sup> which use a very similar concept but employ a much smaller aperture, allowing higher resolution measurements of, e.g., submicron diameter particles. Using these types of sensors, for instance, measurements of very weak binding constants can be achieved by monitoring agglomeration size distributions of small polystyrene beads.<sup>3,4</sup>

A variant approach using optical detection has also been developed, typified by the fluorescence-activated cell sorter, commercial versions of which are available from a number of vendors. An excellent review of this type of instrument appears in the text by Ormerod.<sup>5</sup> This instrument couples the

optical (fluorescent) detection of cells or beads with a sorting mechanism, allowing the separation of particles or cells based on size or fluorescence wavelength.

Microfluidic versions of the Coulter counter, resistive pulse analyzer, and other cell sensing or sorting technologies have also been developed, primarily because such implementations promise very low-cost and disposable instruments, with potentially high throughput.<sup>6–10</sup> A number of these approaches involve electronic sensing techniques, albeit with limited sensitivity and throughput.<sup>7,11–13</sup> Resistive pulse sensing has been achieved with a nanopore fabricated in an elastomer, with nanopore diameters of order a hundred nanometers. By monitoring the electrical resistance of a nanopore through which DNA suspended in saline was passed, it was reported that individual strands of  $\lambda$ -phage DNA could be detected.<sup>14</sup> A broadband dielectric spectrometer, made by placing a coplanar waveguide under, and in line with, an elastomeric microfluidic channel through which different analytes were passed, revealed different signatures when measuring over frequencies from 0 to 25 GHz, although no time-domain response was reported.<sup>13</sup> Time-domain signals, due to passage of cells or particles through an elastomeric or polyimide microfluidic channel, have been generated by monitoring the capacitance at audiofrequencies (1 kHz),<sup>12</sup> or the real and imaginary impedances at frequencies up to 1 MHz,<sup>7,11</sup> sensed by local planar gold electrodes embedded in a 10 to 100  $\mu\text{m}$  diameter channel. These implementations give good sensitivity but relatively low throughput (at most a few tens to hundreds of particles per second). The low-frequency dielectric response due to DNA in or outside of cells yields relatively large signals, and can perhaps be used to identify cells at different points in their reproductive cycle<sup>12,15–18</sup> and can assist in the identification of mutant cells.<sup>19</sup>

Here we describe an approach to the electronic sensing of particles in microfluidic channels, which could eventually provide the basis for cellular electronic characterization. Our

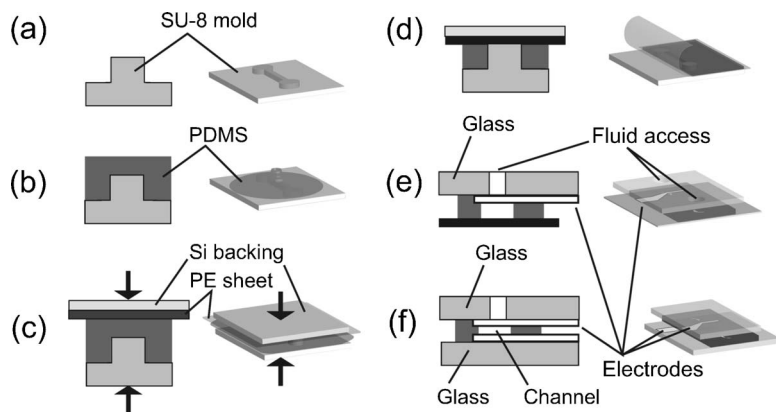


FIG. 1. Device fabrication. (a) An epoxy mold is made using photolithography. (b) Liquid PDMS precursor is poured onto the mold and (c) a fluoropolymer-coated polyethylene (PE) sheet with a silicon substrate backing is placed on top of the PDMS and pressure applied to mold the PDMS. (d) The PDMS is then cured and removed from the mold, using the PE sheet as a handle. (e) A glass substrate with an electrode and fluid access holes is bonded to the surface of the PDMS. (f) The PE sheet is removed, and a glass cover with counterelectrode is bonded to the other PDMS surface.

method is designed to simultaneously achieve high throughput with good size discrimination, a combination that has not been demonstrated previously. We have earlier described a radio-frequency-based cytometer that enabled high-throughput electronic detection of cells and latex beads in a microfluidic system.<sup>20</sup> This device used radiofrequency (rf) read-out of a coplanar electrode, positioned at the base of a  $50 \times 50 \mu\text{m}^2$  cross-section microfluidic channel, to detect particles flowing in saline solution through the channel volume. The presence of particles in the fluid stream perturbs the electric field from the electrodes, which is detected by the corresponding change in the local electrical impedance. One limitation of this device design is that the coplanar electrode geometry generates a highly nonuniform electric sensing field, so that a significant variation in signal strength appears for identical particles passing at different heights over the electrodes. In a uniform electric field, by contrast, the detected signal will not depend on the particle's height and lateral position in the microfluidic channel. Placing the sensing electrodes on opposite sides of the channel (e.g., on the top and bottom), in contrast to the original planar electrode design, would create a much more uniform electric field, allowing a much better discrimination of particles with different size, or differing in other electronic properties.

Here we describe the fabrication and operation of a device with opposed electrodes, implemented through a new fabrication approach using a thin ( $25 \mu\text{m}$ ) poly(dimethyl siloxane) (PDMS) membrane, patterned by molding, sealed between two glass plates, each plate bearing one electrode. Detection was achieved using a significantly improved rf sensing technique, with electronic tuning enabling very high sensitivity and discrimination.<sup>20,21</sup> With this device design, we have demonstrated excellent discrimination between micron-scale polystyrene beads of different diameters, measured at very high flow rates. Beads of a few microns in diameter, that differ in their diameters by less than  $1 \mu\text{m}$ , can easily be distinguished, with signal amplitude distributions comparable to the bead diametric distributions provided by the bead manufacturer, measured using centrifuge-based photodensitometry.

## MATERIALS AND METHODS

### Device fabrication

Microfluidic channels that incorporate opposing electrodes, on either side of the channel, are typically fabricated

by sandwiching a membrane, into which the fluid channel has been defined, between two substrates, each with one electrode patterned on its fluid-contacting side. While such devices have been successfully produced using a glass-polyimide system, the fabrication process is complex and requires tight parameter control.<sup>22</sup> Fluidic chip fabrication using PDMS, by contrast, is robust, inexpensive, and allows rapid prototyping.<sup>23–25</sup> We have devised a new method for fabricating a sealed microfluidic device with opposed electrodes using a PDMS-glass sandwich, employing a simple and easily repeated process. The device fabrication is shown schematically in Fig. 1.

A positive relief mold of the channel structure is prepared by photolithographic patterning of the photodefinable epoxy SU-8 on a silicon substrate.<sup>24</sup> Liquid PDMS precursor is poured onto the mold, and a fluoropolymer-coated polyethylene (PE) sheet<sup>26</sup> is placed on top of the PDMS. A blank silicon wafer is placed on top of the PE sheet, and the structure is mechanically compressed using a mechanical vise, which allows pressures in excess of 1 MPa,<sup>27</sup> sufficient to completely exclude the PDMS from the channel. The PDMS is allowed to partially cure for several hours while under compression, after which the mold is removed from the vise and the PDMS fully cured on a hot plate at  $100 \text{ }^\circ\text{C}$ . When cured, the PDMS will lightly adhere to the fluoropolymer-coated sheet,<sup>28</sup> with enough adhesion to allow the PDMS to be removed from the mold and permitting the sheet to serve as a handle for the PDMS in subsequent process steps.

We patterned Au/Ti (100/10 nm) electrodes on two pieces of soda-lime glass, using standard lift-off photolithography. The glass surfaces were saturated with silanol (SiOH) (Ref. 24) prior to bonding, by soaking in 4:1:2  $\text{H}_2\text{SO}_4:\text{H}_2\text{O}_2:\text{H}_2\text{O}$  at  $80 \text{ }^\circ\text{C}$  for 5 min. This results in very hydrophilic surfaces, indicating good hydrogenation of dangling Si–O bonds. The PDMS surface was prepared by treatment with a UV-ozone photoreactor for 5 min. Fluid inlet and outlet holes were drilled into one of the glass substrates, and this substrate was aligned to the PDMS channel using a flip-chip bonder. After alignment, the membrane was bonded to the substrate by bringing them into conformal contact and heating on a hot plate at  $130 \text{ }^\circ\text{C}$  for 5 min. The PE sheet was then removed from the PDMS to expose the other side of the membrane. The newly exposed PDMS surface was treated with UV ozone for 5 min, and the second glass substrate, with opposing electrode, flip-chip bonded to the PDMS, in

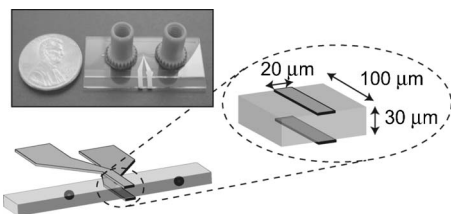


FIG. 2. Schematic of sensor and fluid channel. Inset: Image of completed device with fluidic connections.

registry with the first electrode and the channel in the membrane. The final bonded device was clamped and baked at 130 °C for 2 h. This drives off water and completes the Si–O–Si bond between the PDMS and glass surfaces.<sup>24</sup> Epoxy-based fluidic connections were used to attach tubing to the predrilled holes in the glass substrate. The devices used in this study comprised a fluid channel with  $\approx 25 \times 100 \mu\text{m}^2$  cross section, 5 mm in length, which is addressed using opposing 20  $\mu\text{m}$  wide gold electrodes, which extend across the width of the channel. A completed device is shown in Fig. 2.

### Tuned rf reflectometry measurement

To achieve high-throughput detection, we have implemented a highly sensitive radio frequency reflectometry measurement. The device is embedded in a tunable rf tank circuit, enabling active electronic impedance matching of the device to the 50  $\Omega$  instrumentation.<sup>21,22</sup> The device is tuned to achieve low reflectance, where  $-100$  dB is achievable for short times on a regular basis, corresponding to a 1 part in  $10^5$  impedance match. The presence of a particle in the buffer solution-filled channel produces a change in the local fluid impedance, changing the impedance balance and thus increasing the rf reflectance from the electrodes in the channel. This dark-field scheme gives maximum sensitivity to small changes in the device impedance, while maintaining a large measurement bandwidth (typically  $>10$  MHz). In addition, monitoring the reflectance at high frequencies ( $\sim 100$  MHz) avoids double-layer interfacial impedances and allows sensitive measurement with very small amplitude signals ( $<10$  mV). A schematic of the measurement circuit is shown in Fig. 3. The impedance-matching circuit comprises a series inductor, which phase matches the current and volt-

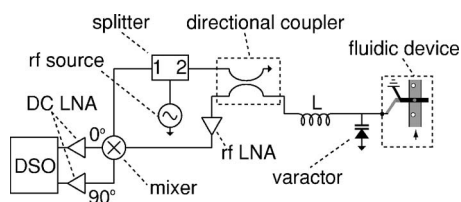


FIG. 3. Radio frequency measurement circuit. A directional coupler couples the rf signal to the load impedance, which comprises the microfluidic device, a shunt varactor for impedance tuning, and a series inductor. Polystyrene beads passing through the detection volume modulate the impedance of the load, changing the amplitude and phase of the reflected rf signal, which is directed to an rf low noise amplifier (rf LNA). The amplified signal is mixed with the original carrier, and the in-phase and quadrature demodulated signals amplified by low noise amplifiers (dc LNA). Signals are acquired for both channels using a digital storage oscilloscope.

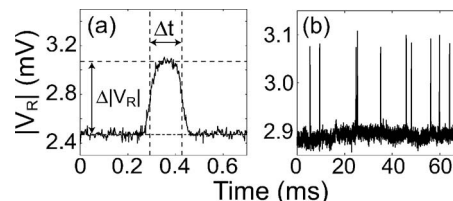


FIG. 4. (a) Bead time trace. Reflected signal amplitude  $|V_R|$  vs time for a single 5.658  $\mu\text{m}$  diameter bead. The change in reflected signal amplitude  $\Delta|V_R|$  is measured from the base line (dot-dashed line) to the peak height, and the transit time  $\Delta t$  is measured at the FWHM (dotted line). (b) Longer time trace of multiple 5.658  $\mu\text{m}$  bead passages, showing roughly a dozen individual events. Beads were measured at a concentration of  $2.5 \times 10^5/\text{ml}$  in PBS at a flow rate of 2 ml/h, and the measurement bandwidth was 300 kHz.

age on the load and a shunt varactor, which allows voltage tuning of the capacitance to ground. We collect both in-phase and quadrature components of the signal, from which can we reconstruct the full reflected wave vector (amplitude and phase). The final stage amplifiers include selectable low-pass filters, which are used to control the measurement bandwidth. All measurements were performed in unit strength phosphate buffer saline (PBS), with the device typically impedance matched to  $-40$  dB reflectance or better, with a  $-20$  dBm (2.2 mV) excitation signal in the range of 105–108 MHz.

### Particle discrimination

We evaluated the ability of this device to distinguish particles by measuring the response to polystyrene beads of different diameters. Solutions of beads with  $4.452 \pm 0.127$ ,<sup>29</sup>  $5.658 \pm 0.305$ ,<sup>29</sup>  $7.320 \pm 0.53$ ,<sup>30</sup> and  $9.016 \pm 0.80$ <sup>30</sup>  $\mu\text{m}$  diameters were obtained and diluted in PBS for measurement. We measured pure samples of individual bead diameters and compared the measured distribution of signal responses with the bead size distribution from the manufacturer. In addition, we measured mixtures of bead sizes at moderate flow rates and concentrations to demonstrate the ability to discriminate beads. We also measured mixtures of two bead sizes at high flow rates and concentrations, to demonstrate high-throughput discrimination.

## RESULTS AND DISCUSSION

The passage of a bead in the sensing volume of the microfluidic channel changes the reflected signal from the reflectometer, which is recorded as a demodulated time-dependent voltage. Figure 4(a) shows a time trace measured for an individual 4.452  $\mu\text{m}$  diameter bead flowing through the detector at 2 ml/h. The signal from the bead is clearly resolved with good signal to noise, giving a clear measurement of the signal amplitude  $\Delta|V_R|$  as well as the transit time  $\Delta t$ , the latter agreeing well with the flow rate. On longer time scales, the signals from multiple beads give signal amplitudes that fall into a narrow range of values, as shown in Fig. 4(b), allowing discrimination of beads based on their size.

Histograms were accumulated for each bead diameter used, yielding a calibration of signal amplitude for each diameter. Figure 6 shows histograms of the signal response  $\Delta|V_R|$  for pure populations of each individual bead size. For

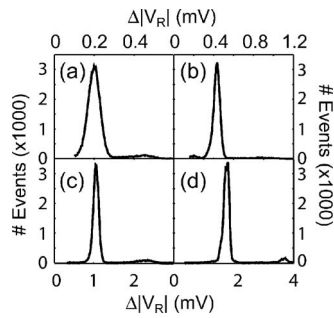


FIG. 5. Histograms of signal amplitudes for pure bead samples, showing number of events vs signal amplitude for pure samples of beads with diameters of (a) 4.452, (b) 5.658, (c) 7.320, and (d) 9.016  $\mu\text{m}$ . Beads were measured at a concentration of  $\sim 2.5 \times 10^5/\text{ml}$  in PBS at a flow rate of 3 ml/h. Each histogram represents  $>30\,000$  events; bin sizes are 10, 16, 16, and 25  $\mu\text{V}$  for (a), (b), (c), and (d) respectively. Additional peaks are due to doublet events.

each size of bead measured, there is a large dominant peak and a smaller peak at twice the main peak amplitude, which indicates measurement of two beads simultaneously due either to random concurrence of beads in the sensing volume or due to bead aggregation. We have excluded bead concurrency as the cause by considering the statistical likelihood of these events. We assume a random distribution of beads, where the probability for concurrent events is given by a Poisson distribution

$$P_k(\tau) = \frac{e^{-\lambda\tau}(\lambda\tau)^k}{k!}, \quad (1)$$

where  $k$  is the number of concurrent beads,  $\lambda$  is the bead concentration, and  $\tau$  is the sensing volume. Given an average bead concentration of  $2.5 \times 10^5$  beads/ml and a sensing volume of 60 pl, we expect that two beads arriving simultaneously in the sensor volume will account for  $\sim 0.01\%$  of all events. We observe that double-amplitude events account for 4.5% of the total events in the histogram of 9.016  $\mu\text{m}$  beads [Fig. 5(d)], more than two orders of magnitude higher than indicated by random concurrence, and more likely due to agglomeration in the source material. Doublet formation due to bead aggregation has been verified by optical inspection of beads in PBS working solution. Hydrophobic aggregation of polystyrene beads in aqueous solutions is a known problem, and it is exacerbated by the PBS working solution, whose free ions screen the native charges on the beads. Additionally, a spurious low amplitude signal is observed in the histogram of 5.658  $\mu\text{m}$  diameter beads [Fig. 5(b)], which is due to a small population of  $\sim 4.5$   $\mu\text{m}$  diameter beads, as verified by the manufacturer's characterization of this bead lot.<sup>31</sup> The measured signal spreads of single bead events for 4.452, 5.658, 7.32, and 9.016  $\mu\text{m}$  diameter beads were 16%, 13%, 8%, and 8%, respectively, comparable to the spreads in the manufacturers' specifications. We believe some of the spread could be eliminated by further modifying the electrode geometry. Finite element simulations indicate that the electric field, measured as a function of height in the channel from the electrode midpoint, varies by about 9% from the electrode surface to the channel center, significantly less than in the coplanar geometry, but still not negligible. The electric field nonuniformity could be decreased further by increasing

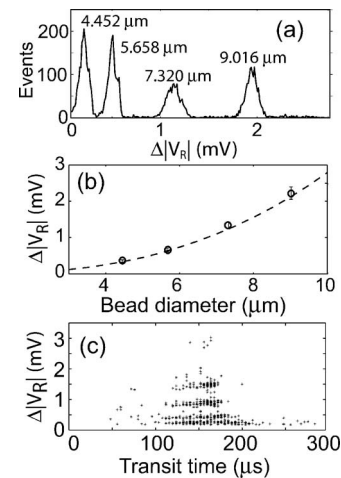


FIG. 6. Measurement of mixtures of polystyrene beads with 4.452, 5.658, 7.320, and 9.016  $\mu\text{m}$  average diameters. (a) Histogram of signal amplitudes, with bin size of 12.5  $\mu\text{V}$ . (b) Mean signal amplitude vs bead diameter. The open circles are measured signal mean with standard deviation given by error bars. The dashed curve is a fit to  $\Delta|V_R| \propto d^{2.6}$ , where  $d$  is the bead diameter. (c) Signal amplitude vs transit time. Beads were measured at a concentration of  $2.5 \times 10^5/\text{ml}$  in PBS, with flow rate of 3 ml/h and a 10 kHz measurement bandwidth.

the width of the electrodes relative to the channel height; doubling the electrode width for the same height channel would reduce the electric field variation by an order of magnitude, and quadrupling the sensor width would reduce it by a factor of 100. This could be done without significantly increasing the likelihood of concurrent bead events. At a concentration of  $2.5 \times 10^5$  beads/ml, quadrupling the sensor width, to 80  $\mu\text{m}$ , would only cause concurrence in 0.2% of the events.

The ability to distinguish bead diameter by signal amplitude was evaluated by measuring mixtures of beads. Figure 6(a) shows a signal amplitude histogram for a mixture of 4.452, 5.658, 7.32, and 9.016  $\mu\text{m}$  diameter beads flowing through the detector at 3 ml/h. The overall bead concentration was  $\sim 2.5 \times 10^5/\text{ml}$ , with roughly equal number concentrations of each bead size. Individual bead sizes are clearly indicated by large, well-separated peaks in the histogram. Average throughput during 40 s of measurement was 173 beads/s, which is more than an order of magnitude higher than the best prior electronic cytometer report of 16 beads/s.<sup>32</sup> Doublet formation in the mixed bead sample generates signals at twice the single bead amplitudes, as well as at other amplitudes for doublets of different sized beads, and these doublet combinations appear to explain all the anomalous peaks in the distribution.

We evaluated the relation between signal amplitude and bead diameter  $d$ , as shown in Fig. 6(b). We found that  $\Delta|V_R| \propto d^{2.6}$ , where  $\Delta|V_R|$  is the average voltage change. The resistance and capacitance change of a block of conducting fluid, that includes a small embedded dielectric sphere, will vary with the sphere volume, i.e., in proportion to the diameter cubed.<sup>33,34</sup> The measured dependence deviates slightly from this prediction, with a lower power than expected (2.6 versus 3). The calculations, however, assume that the embedded sphere is small in comparison to the fluid dimensions, so that the sphere only perturbs the electric field

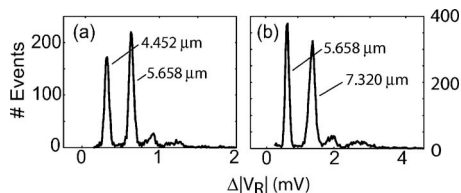


FIG. 7. High-throughput bead discrimination. Histograms of signal amplitude for mixtures of (a) 4.452 and 5.658  $\mu\text{m}$  and (b) 5.658 and 7.320  $\mu\text{m}$  diameter beads. Bead concentration was  $\sim 2.5 \times 10^6/\text{ml}$  in PBS, at a flow rate of 10 ml/h, with a 30 kHz measurement bandwidth. Measured throughputs were (a) 4890 and (b) 5010 beads/s, and bin sizes were (a) 20 and (b) 30  $\mu\text{V}$ . Additional peaks due to bead doublets.

slightly. In our study, the largest beads represent a significant fraction of the sensing volume, and therefore perturb the electric field significantly, possibly accounting for the observed discrepancy.

As shown in Fig. 4, the bead transit time across the sensor can also be used as a metric to analyze bead transport. Figure 6(c) shows signal amplitude plotted against transit time for the range of bead diameters studied. All bead diameters give very close to the same average transit time  $\Delta t$ , although the smaller beads give a larger scatter in the transit time than do the larger beads. The transit time, measured as the full width at half maximum for each individual bead, is independent of the bead diameter, indicating that the bead velocity is likely determined solely by the fluid velocity, and that bead position in the channel does not depend on bead diameter, as otherwise the Poiseuille flow pattern would generate a systematic dependence.

We used the large measurement bandwidth to distinguish beads by signal amplitude at very high throughput. Figure 7 shows a measurement of a 4.452 and 5.658  $\mu\text{m}$  bead mixture, and separately 7.320  $\mu\text{m}$  mixed with 9.016  $\mu\text{m}$  diameter beads, at a throughput of  $\approx 5000$  beads/s, more than two orders of magnitude faster than previous electronic measurements.<sup>32</sup> Background from doublet events contaminates these distributions as well, but the main peaks are still clearly distinguished. As the concentration of beads is increased, random concurrence of beads in the sensing volume, as opposed to bead aggregation events, also becomes more prevalent. Assuming a random bead distribution, we predict that at this concentration, two concurrent beads should represent  $\approx 1\%$  of the total event population, while double-amplitude events in Fig. 7(a) actually represent 14% of the total population of 5.658  $\mu\text{m}$  beads, clearly indicating strong aggregation. Throughput could be increased even further by increasing the solution flow rate, keeping the bead concentration constant. Note that the measurement has an intrinsic bandwidth of 10 MHz, so that we are not even close to the upper limit set by the measurement.

## CONCLUSIONS

We have developed a new fabrication technique, which allows fabrication of an opposing electrode sensor using PDMS microchannels, using an approach that is simpler and more robust than the equivalent polyimide-based approach.<sup>22</sup> We have also developed a high bandwidth, very high sensitivity rf detection technique,<sup>20,21</sup> using a tuning varactor as a

critical impedance-matching element, with which we are able to achieve significantly increased throughput compared to earlier work.<sup>32,35</sup> We have demonstrated the ability to distinguish particles with diameters differing by 1  $\mu\text{m}$  at a throughput of 5000 beads/s, i.e., more than  $15 \times 10^6$  beads/hour, more than two orders of magnitude faster than previous studies.<sup>32</sup> We plan to improve the sensor geometry, focusing on improving electric field uniformity. In addition we intend to incorporate a second electrode set, which will allow an independent measurement of particle velocity. This approach might form the basis for label-free detection and discrimination of biological cells, or possibly used for molecular assays.

## ACKNOWLEDGMENTS

This work was supported in part by the NIH through an NIH PEN grant and by the DMEA/DARPA Center for Nanoscience Innovation for Defence.

- <sup>1</sup>W. H. Coulter, U. S. Patent No. 2656508 (1953).
- <sup>2</sup>R. W. de Blois and C. P. Bean, Rev. Sci. Instrum. **41**, 909 (1970).
- <sup>3</sup>G. K. von Schulthess and G. B. Benedek, Macromolecules **13**, 939 (1980).
- <sup>4</sup>G. K. von Schulthess and G. B. Benedek, Macromolecules **16**, 434 (1983).
- <sup>5</sup>M. G. Ormerod, *Flow Cytometry: A Practical Approach* (Oxford University Press, Oxford, 1994).
- <sup>6</sup>A. G. J. Tibbe, B. G. de Groot, J. Greve, G. J. Dolan, C. Rao, and L. W. M. M. Terstappen, Cytometry **47**, 163 (2002).
- <sup>7</sup>S. Gawad, K. Cheung, U. Seger, A. Bertsch, and P. Renaud, Lab Chip **4**, 241 (2004).
- <sup>8</sup>M. Berger, J. Castelino, R. Huang, M. Shah, and R. H. Austin, Electrophoresis **22**, 38833892 (2001).
- <sup>9</sup>M. Dürr, J. Kentsch, T. Müller, T. Schnelle, and M. Stelzle, Electrophoresis **24**, 722 (2003).
- <sup>10</sup>M. M. Wang, E. Tu, D. E. Raymond, J. M. Yang, H. C. Zhang, N. Hagen, B. Dees, E. M. Mercer, A. H. Forster, I. Kariv, P. J. Marchand, and W. F. Butler, Nat. Biotechnol. **23**, 83 (2005).
- <sup>11</sup>S. Gawad, L. Schild, and P. Renaud, Lab Chip **1**, 76 (2001).
- <sup>12</sup>L. L. Sohn, O. A. Saleh, G. R. Facer, A. J. Beavis, R. S. Allan, and D. A. Notterman, Proc. Natl. Acad. Sci. U.S.A. **97**, 10687 (2000).
- <sup>13</sup>G. R. Facer, D. A. Notterman, and L. L. Sohn, Appl. Phys. Lett. **78**, 996 (2001).
- <sup>14</sup>O. A. Saleh and L. L. Sohn, Nano Lett. **3**, 37 (2003).
- <sup>15</sup>K. Asami and T. Yonezawa, Biochim. Biophys. Acta **1245**, 99 (1995).
- <sup>16</sup>K. Asami, E. Gheorghiu, and T. Yonezawa, Biophys. J. **76**, 3345 (1999).
- <sup>17</sup>X. J. Wang, F. F. Becker, and P. R. C. Gascoyne, Biochim. Biophys. Acta **1564**, 412 (2002).
- <sup>18</sup>K. Asami, J. Phys. D **39**, 4656 (2006).
- <sup>19</sup>K. Asami and T. Yonezawa, Biophys. J. **71**, 2192 (1996).
- <sup>20</sup>D. K. Wood, S.-H. Oh, S.-H. Lee, H. T. Soh, and A. N. Cleland, Appl. Phys. Lett. **87**, 184106 (2005).
- <sup>21</sup>D. K. Wood, G. B. Braun, J. L. Fraikin, L. J. Swenson, N. O. Reich, and A. N. Cleland, Lab Chip **4**, 469 (2007).
- <sup>22</sup>S. Metz, R. Holzer, and P. Renaud, Lab Chip **1**, 29 (2001).
- <sup>23</sup>Y. Xia, E. Kim, X. M. Zhao, J. A. Rogers, M. Prentiss, and G. M. Whitesides, Science **273**, 347 (1996).
- <sup>24</sup>D. C. Duffy, J. C. McDonald, O. J. A. Schueller, and G. M. Whitesides, Anal. Chem. **70**, 4974 (1998).
- <sup>25</sup>D. C. Duffy, O. J. A. Schueller, S. T. Brittain, and G. M. Whitesides, J. Micromech. Microeng. **9**, 211 (1999).
- <sup>26</sup>Scotchpak 1020, 3M, St. Paul, MN.
- <sup>27</sup>J. R. Anderson, D. T. Chiu, R. J. Jackman, O. Cherniavskaya, J. C. McDonald, H. Wu, S. H. Whitesides, G. M. Whitesides, Anal. Chem. **72**, 3158 (2000).
- <sup>28</sup>C. Neils, Z. Tyree, B. Finlayson, and A. Folch, Lab Chip **4**, 342 (2004).
- <sup>29</sup>Polybead, Polysciences, Warrington, PA.
- <sup>30</sup>Uniform Polystyrene Microspheres, Bangs Laboratories, Fishers, IN.

- <sup>31</sup> Polybead catalog No. 07312 and lot No. 551628 measured by high speed disk centrifuge photodensitometer, Polysciences, Warrington, PA.
- <sup>32</sup> K. Cheung, S. Gawad, and P. Renaud, *Cytometry Part A* **65A**, 124 (2005).
- <sup>33</sup> J. Israelachvili, *Intermolecular and Surface Forces*, 2nd ed. (Academic

Press, New York, 1992).

- <sup>34</sup> M. Koch, A. G. R. Evans, and A. Brunnschweiler, *J. Micromech. Microeng.* **9**, 159 (1999).
- <sup>35</sup> S. Gawad, L. Schild, and P. Renaud, *Lab Chip* **1**, 76 (2001).